

Photosynthetic maximum quantum yield increases are an essential component of the Southern Ocean phytoplankton response to iron

Michael R. Hiscock^{†‡§}, Veronica P. Lance[‡], Amy M. Apprill[¶], Robert R. Bidigare[¶], Zackary I. Johnson[¶], B. Greg Mitchell[¶], Walker O. Smith, Jr.^{††}, and Richard T. Barber[‡]

[†]Program in Atmospheric and Oceanic Sciences, Princeton University, 300 Forrestal Campus, Princeton, NJ 08544; [‡]Duke University Nicholas School of the Environment and Earth Sciences, 135 Duke University Marine Lab Road, Beaufort, NC 28516; [¶]Department of Oceanography, University of Hawaii at Manoa, 1000 Pope Road, Honolulu, HI 96822; [§]Scripps Institution of Oceanography, University of California at San Diego, 9500 Gilman Drive, La Jolla, CA 92093; and ^{††}Virginia Institute of Marine Sciences, College of William and Mary, Gloucester Point, VA 23062

Edited by William H. Schlesinger, The Institute of Ecosystem Studies, Millbrook, NY, and approved December 10, 2007 (received for review May 28, 2007)

It is well established that an increase in iron supply causes an increase in total oceanic primary production in many regions, but the physiological mechanism driving the observed increases has not been clearly identified. The Southern Ocean iron enrichment experiment, an iron fertilization experiment in the waters closest to Antarctica, resulted in a 9-fold increase in chlorophyll (Chl) concentration and a 5-fold increase in integrated primary production. Upon iron addition, the maximum quantum yield of photosynthesis (ϕ_m) rapidly doubled, from 0.011 to 0.025 mol C·mol quanta⁻¹. Paradoxically, this increase in light-limited productivity was not accompanied by a significant increase in light-saturated productivity (P_{max}^b). P_{max}^b , maximum Chl normalized productivity, was 1.34 mg C·mg Chl⁻¹·h⁻¹ outside and 1.49 mg C·mg Chl⁻¹·h⁻¹ inside the iron-enriched patch. The importance of ϕ_m as compared with P_{max}^b in controlling the biological response to iron addition has vast implications for understanding the ecological response to iron. We show that an iron-driven increase in ϕ_m is the proximate physiological mechanism affected by iron addition and can account for most of the increases in primary production. The relative importance of ϕ_m over P_{max}^b in this iron-fertilized bloom highlights the limitations of often-used primary productivity algorithms that are driven by estimates of P_{max}^b but largely ignore variability in ϕ_m and light-limited productivity. To use primary productivity models that include variability in iron supply in prediction or forecasting, the variability of light-limited productivity must be resolved.

climate change | iron fertilization | primary production | high-latitude photophysiology | photochemical efficiency

Dozen iron enrichment experiments in high-nutrient low-chlorophyll (Chl) regions of the world ocean have unequivocally shown that iron limits primary production and that the addition of iron has significant biogeochemical consequences (1, 2). Although it has been shown that enhanced iron supply increases biomass, photosynthetic efficiency and primary production within the entire phytoplankton assemblage (3–6), the photophysiological mechanism driving the increased productivity has not been analytically linked to the observed changes in protein expression and photochemistry (7). On the most basic level, phytoplankton photosynthesis can be categorized as either light-limited photosynthesis or light-saturated photosynthesis (8). At low irradiances, the rate of phytoplankton photosynthesis is light limited and proportional to the supply of irradiance. As irradiance increases, photosynthesis increases proportionally until the photosynthetic capabilities of the phytoplankton begin to become saturated. Light-saturated photosynthetic rates then remain constant as irradiance levels increase.

Here, we show that iron addition results in a doubling of light-limited photosynthesis rates but has no statistically significant impact on light-saturated photosynthesis rates. These re-

sults shed light on the mechanistic response to iron addition. Iron limitation decreases light-limited photosynthesis primarily by reducing the ability of phytoplankton to synthesize functional proteins for *de novo* creation or repair of damaged reaction centers (7). In particular, photosynthetic reaction center core and electron transport chain proteins that require iron cannot be formed or repaired, resulting in a reduced ability to process absorbed light energy into chemical energy. Under iron limitation, damaged photosystem II reaction centers manifest as decreased variable fluorescence, and a lesioned electron transport results in a decreased reaction center turnover rate (7, 9). Both processes directly reduce light-limited photosynthesis, ultimately resulting in a reduction in the quantum yield of photosynthesis (10).

In this context we explore (i) the strong ecological importance of light-limited photosynthesis, (ii) the implications of these results for primary production models that are primarily modulated by parameters that describe light-saturated photosynthesis, and (iii) the need for models to have the ability to represent changes in light-limited photosynthesis. We briefly describe the Southern Ocean iron enrichment experiment (SOFeX). We then introduce standard primary production models, the photosynthetic efficiency results from SOFeX, and an example of a primary production model that has the capacity to resolve increases in primary productivity caused by iron-dependent changes in the efficiency of light-limited photosynthesis.

Results and Discussion

SOFeX. The SOFeX group conducted an *in situ* iron fertilization in January and February 2002 in the Pacific Sector of the Southern Ocean, one of a series of experiments designed to test the Martin Iron Hypothesis (11). The southern of the two SOFeX patches (1) was in the waters nearer Antarctica and poleward of the southern boundary of the Antarctic circumpolar current ($\approx 66^\circ\text{S}$, 172°W). One of three major high-nutrient, low-Chl regions of the world ocean, these waters were characterized by high levels of macronutrients ($\approx 28 \mu\text{M}$ nitrate, $60 \mu\text{M}$ silicic acid) (12), extremely low iron concentrations (13, 14), iron-limited production (15), well defined mixed layers (45 m), and cold surface temperatures (-0.5°C) (1). Acidified iron sulfate was mixed with ambient seawater and introduced just

Author contributions: M.R.H., Z.I.J., B.G.M., W.O.S., and R.T.B. designed research; M.R.H., V.P.L., A.M.A., R.R.B., and R.T.B. performed research; M.R.H. analyzed data; and M.R.H., V.P.L., Z.I.J., and R.T.B. wrote the paper.

The authors declare no conflict of interest.

This article is a PNAS Direct Submission.

Freely available online through the PNAS open access option.

[§]To whom correspondence should be addressed. E-mail: mhiscock@princeton.edu.

© 2008 by The National Academy of Sciences of the USA

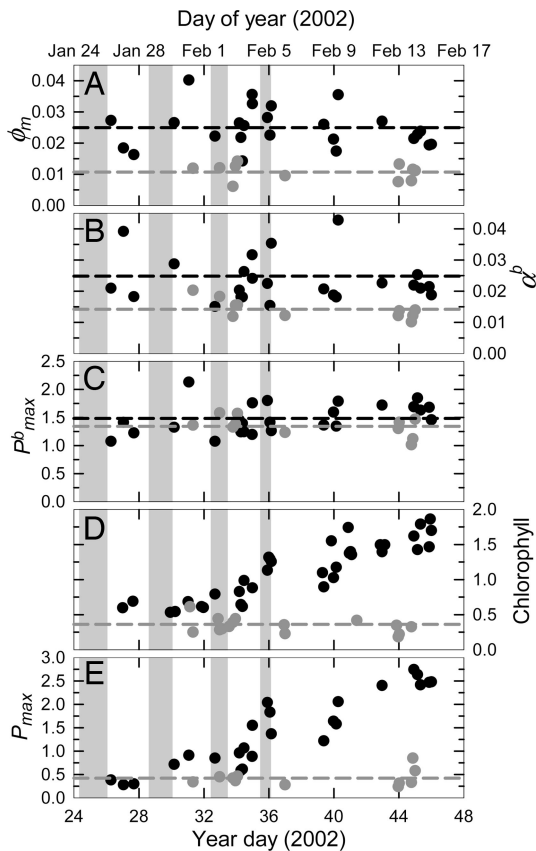


Fig. 1. Time series of phytoplankton physiological parameters [ϕ_m , maximum quantum yield (A); α^b , maximum Chl-specific light utilization coefficient (B); P_{max}^b , Chl-specific maximum primary productivity (C)], biomass [HPLC-derived Chl (D)], and primary productivity [P_{max} , maximum primary productivity (E)]. Black circles and black dotted lines represent discrete samples and the mean value inside the iron-enriched patch, respectively. Dark gray circles and dark gray dotted lines represent discrete samples and mean values outside the iron-enriched patch, respectively. Gray bars indicate periods of iron fertilization. Physiological units are as in Table 1: P_{max} ($\text{mgC} \cdot \text{m}^{-3} \cdot \text{h}^{-1}$), chlorophyll (mg m^{-3}).

below the sea surface into a $\approx 15\text{-km} \times 15\text{-km}$ patch over 2 days, resulting in a surface iron concentration of ≈ 0.7 nM dissolvable Fe. The patch was fertilized three additional times (Fig. 1, gray bars) and responses were monitored for 27 days.

Primary Productivity Models. Primary productivity models have appeared in the literature on average once every 2 years over the past four decades (16). Recent reviews conclude that after reconciling numerous aliases for similar parameters and differing complexities of spectral light integration, primary productivity models are fundamentally the same (16–18). Behrenfeld and Falkowski (16) described a standard depth-integrated model (DIM),

$$PP_{eu} = Chl_0 \cdot Z_{eu} \cdot P_{opt}^b \cdot DL \cdot F, \quad [1]$$

where total daily primary productivity within the euphotic zone (PP_{eu}) is equal to surface Chl (Chl_0) scaled to the depth of the euphotic zone (Z_{eu}) multiplied by the Chl-specific optimal photosynthetic rate (P_{opt}^b) scaled to day length (DL) times a light limitation term (F). Note that P_{opt}^b is operationally distinct from P_{max}^b , which describes the Chl-normalized light-saturated rate of photosynthesis as controlled by the cellular concentration and activity of dark reaction enzymes and can be measured in the laboratory with 2-h photosynthesis versus irradiance (PvsE) exper-

iments. P_{opt}^b , which is measured in the field, is the optimal Chl-normalized, light-saturated rate of photosynthesis as governed by the counterbalancing effects of light limitation, light saturation, and photoinhibition over a 24-h period. Although P_{opt}^b and P_{max}^b are operationally distinct, they are functionally similar in that they predominantly describe light-saturated photosynthesis.

The variables in Eq. 1 are ranked in importance according to their ecological variability in Behrenfeld and Falkowski's consumer's guide to phytoplankton primary productivity models (16). Most of the three orders of magnitude change in PP_{eu} ($\approx 30\text{--}10,000$ $\text{mg C} \cdot \text{m}^{-2} \cdot \text{d}^{-1}$) is the result of 250-fold depth-integrated changes in phytoplankton biomass, $Chl_0 \cdot Z_{eu}$ ($\approx 2\text{--}500$ $\text{mg Chl} \cdot \text{m}^{-2}$). P_{opt}^b varies within a factor of 40 ($\approx 0.5\text{--}20$ $\text{mg C} \cdot \text{mg Chl}^{-1} \cdot \text{h}^{-1}$), and estimates of the dimensionless F indicate it can potentially cause PP_{eu} to change by a factor of ≈ 4 . DL has only a minor effect on the variability of PP_{eu} .

This ranking has been demonstrated statistically. In a compilation of $>11,000$ ^{14}C measurements of primary productivity, 38% of the observed variability in PP_{eu} was accounted for solely by the product of surface Chl (Chl_0) and euphotic depth (Z_{eu}) (17). When measured values of P_{opt}^b were used in Eq. 1 the correlation improved to 86% (17). Alternatively, in that study the light-limitation variable F in Eq. 1 made little difference to the model output. In their study, Behrenfeld and Falkowski (16) developed and used a simple light-dependent equation to represent F :

$$F = \frac{0.66125 \cdot E_d(0^+)}{E_d(0^+) + 4.1}, \quad [2]$$

where F is dimensionless and ranges between 0.45 and 0.61 for $E_d(0^+)$, total daily irradiance just above the surface of the ocean, values from 9 to 60 $\text{mol quanta} \cdot \text{m}^{-2} \cdot \text{d}^{-1}$. With this empirical representation of F and observed measures of Chl_0 , Z_{eu} , and P_{opt}^b , the correlation between modeled and measured productivity was 86%. Furthermore, model performance decreased by only 3% ($r^2 = 0.83$) when F was held constant at an average value of 0.55 (16).

This robust analysis marginalizes the use of light-limited photosynthesis parameters within production algorithms. Behrenfeld and Falkowski (16, 17) argued that productivity algorithm performance primarily depends on the accuracy to which P_{opt}^b can be modeled. Furthermore, they argued that adding computational overhead in the form of complex light propagation models adds limited, if any, increase in model performance. In a recent primary-productivity-algorithm-testing round robin there were 23 of 24 algorithms within the study that included variable phytoplankton physiology (19). Only six of those 23 algorithms included a light-limitation term that was based on physiology rather than scaled to daily mean irradiance (i.e., Eq. 2). In 13 of the algorithms, variations in phytoplankton physiology were limited to variations in P_{opt}^b or P_{max}^b . It was also noted that one of the most widely used algorithms is the vertically generalized production model (17), a combination of Eqs. 1 and 2, in which P_{opt}^b is obtained as a seventh-order polynomial of sea surface temperature.

In this article we revisit the importance of light-limited productivity. We show that in this Southern Ocean iron enrichment 5-fold integrated primary productivity and 9-fold Chl concentration increases (4) were not accompanied by a significant increase in P_{max}^b . Instead, productivity and biomass increases were driven by 2-fold increases in α^b and ϕ_m , measures of the efficiency of light-limited productivity and components of the productivity model variable F . The standard DIM proposed by Behrenfeld and Falkowski (16, 17), a combination of Eqs. 1 and 2, would fail to model the development of an iron-enriched bloom because the proximal physiological drivers of the productivity increase (α^b , ϕ_m) are not model inputs. By showing that

Table 1. Phytoplankton physiological parameters and single factor ANOVA significance test of out vs. in of the iron-enriched patch (25 in samples, 11 out samples)

Parameter	Units	Location	Mean	SE	Min	Max	P value	Significance
ϕ_m	mol C·mol quanta ⁻¹	Out	0.011	±0.001	0.006	0.014	3.9E-8	***
		In	0.025	±0.001	0.014	0.040		
P_{max}^b	mg C·mg Chl ⁻¹ ·h ⁻¹	Out	1.34	±0.05	1.01	1.58	0.1190	ns
		In	1.49	±0.05	1.07	2.13		
α^b	mg C·mg Chl ⁻¹ ·h ⁻¹ ·μmol quanta·m ⁻² ·s ⁻¹	Out	0.014	±0.001	0.010	0.020	0.0011	**
		In	0.025	±0.002	0.015	0.056		
E_k	μmol quanta·m ⁻² ·s ⁻¹	Out	97	±4	67	111	3.8E-6	***
		In	65	±3	36	92		
$\bar{a}_{\phi_{INC}}^*$	m ² mg Chl ⁻¹	Out	0.032	±0.002	0.024	0.045	0.0022	**
		In	0.023	±0.001	0.016	0.049		

ns = not significant. Significance: *, 0.01 < P ≤ 0.05; **, 0.001 < P ≤ 0.01; ***, P ≤ 0.001.

productivity increases observed during SOFeX were driven by increases in α^b and ϕ_m , we underscore the limitations of using light-saturated (P_{max}^b - or P_{opt}^b -based) production models and the importance of using the family of models that resolve light-limited production (e.g., refs. 20–22). Models that account for variability in light-limited photosynthesis will better reproduce the effects of natural background and episodic iron input.

SOFeX Results. There was an immediate and sustained increase in the maximum quantum yield (ϕ_m) of total phytoplankton in response to iron addition (Fig. 1A). ϕ_m is the fundamental quotient of the moles of carbon incorporated in the phytoplankton cell divided by the moles of light that the phytoplankton cell absorbs and is a key indicator of the photosynthetic efficiency of phytoplankton. The >2-fold mean increase in ϕ_m (Table 1) was driven by a nearly 2-fold increase in the maximum light utilization coefficient, α^b (Table 1 and Fig. 1B), and a 28% decrease in the mean absorption normalized to incubator irradiance, ($\bar{a}_{\phi_{INC}}^*$) (Table 1). The increases in photosynthetic efficiency of light-limited production, α^b and ϕ_m , were not accompanied by a statistically significant increase in P_{max}^b (Fig. 1C and Table 1).

Throughout the iron enrichment experiment, Chl accumulated and primary productivity increased (Fig. 1D and E). It is important to note that the increases in Chl resulted from a proportionally similar increase within the pico-, nano-, and micro-phytoplankton size classes (Fig. 2A). Iron addition did not markedly change the proportional makeup of the phytoplankton size-fraction assemblage. Likewise, whereas the absolute concentrations of the photosynthetic carotenoids (PCs) peridinin, 19'-butanoyloxyfucoxanthin, fucoxanthin, and 19'-hexanoyloxyfucoxanthin increased ≈2-fold with iron addition, the PC:Chl quotients were similar inside and outside the iron-enriched patch (Fig. 2B). Fucoxanthin, a marker for diatoms, was the dominant PC inside and outside the iron-enriched patch, and the Chl-normalized relationships among the PCs changed very little (Fig. 2B).

Because there was no significant increase in the performance of light-saturated maximum productivity (P_{max}^b) and the proportion of pigments and size classes within the phytoplankton assemblage changed very little, we argue that the observed increases in Chl and productivity were primarily the result of increased photosynthetic efficiency in light-limited productivity (α^b). Primary productivity models that do not include light-limited photosynthesis parameters such as α^b and ϕ_m cannot model this productivity response to iron addition. The following light-limited-photosynthesis-resolving productivity model demonstrates that, by primarily increasing the efficiency of light-limited photosynthesis, significant increases in primary productivity can be achieved.

Productivity Model Using SOFeX Results. There is a diversity of primary productivity models that build in complexity on the standard DIM presented in Eq. 1. With some minor exceptions (i.e., changes in Chl and P_{opt}^b with depth) the overriding difference between the DIM presented in Eq. 1 and more complicated depth-, time- and wavelength-resolved models is the treatment of the propagation of light through the water column and the expression of the efficiency of light-limited productivity (ϕ_m , α^b). In Eq. 1 the treatment of irradiance, α^b and ϕ_m is expressed within the dimensionless variable F . Because it is thought that F plays a relatively minor role in the overall global variability of PP_{eu} , most models of primary productivity use an average value

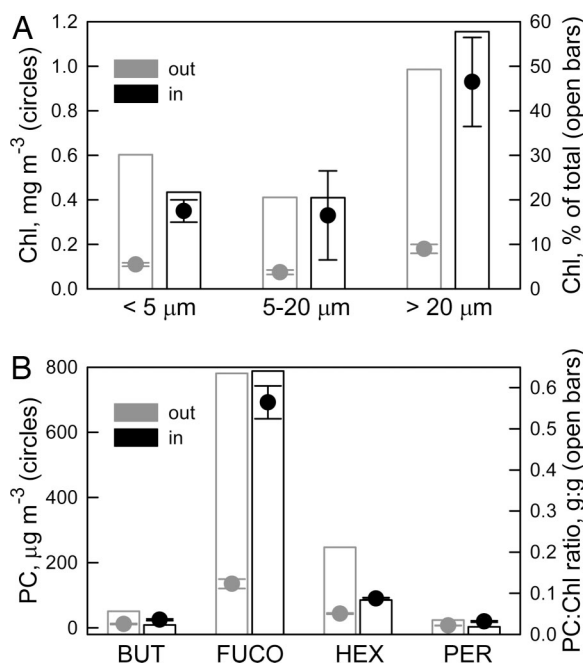


Fig. 2. PC pigments and size-fractionated Chl. (A) Size-fractionated fluorometrically derived Chl concentrations outside (gray circles) and inside (black circles) the iron-enriched patch. Gray and black open bars are a proportional representation of each of the three size classes outside and inside the iron-enriched patch, respectively. (B) HPLC-determined PC concentrations (circles) and PC:Chl quotients (open bars). Out values (gray) are means for the entire experimental period. In values (black) represent means of the three, inside the patch, stations with the highest primary productivity (4). Error bars are SEM. <5 μm, picoplankton; 5–20 μm, nanoplankton; >20 μm, microplankton; PER, peridinin; BUT, 19'-butanoyloxyfucoxanthin; FUCO, fucoxanthin; HEX, 19'-hexanoyloxyfucoxanthin.

of F or vary F as a function of light, as in Eq. 2. However, to resolve the observed iron-dependent 2-fold changes in α^b and ϕ_m it is necessary to use a productivity model that expresses F and light-limited primary productivity more fully.

A typical light-limited, photosynthesis-resolving productivity model resolves the quantity and quality of irradiance throughout the water column and throughout the day (see review in ref. 18). In this case the resolution is 1 m and ≈ 30 s:

$$PP_{eu} = \int_{0m}^{Z_{eu}} \int_{\text{sunrise}}^{\text{sunset}} P_{\max}^b \cdot Chl(z) \cdot \tanh \left[\frac{\phi_m \bar{a}_{\phi PUR}^*(z) \cdot E_0(z, t) \cdot 43.2}{P_{\max}^b} \right] dt dz, \quad [3]$$

where PP_{eu} is the daily primary productivity integrated to the depth of the euphotic zone ($\text{mg C} \cdot \text{m}^{-2} \cdot \text{d}^{-1}$); P_{\max}^b is the maximum Chl-specific productivity ($\text{mg C} \cdot \text{mg Chl} \cdot \text{h}^{-1}$); $Chl(z)$ is the depth-dependent Chl concentration ($\text{mg Chl} \cdot \text{m}^{-3}$); ϕ_m is the maximum quantum yield ($\text{mol C} \cdot \text{mol quanta}^{-1}$); $E_0(z, t)$ are 30-s and 1-m intervals of irradiance ($\mu\text{mol quanta} \cdot \text{m}^{-2} \cdot \text{s}^{-1}$); 43.2 converts micromols and milligrams to moles and hours to seconds; and $\bar{a}_{\phi PUR}^*(z)$ is the mean Chl-specific absorption coefficient ($\text{m}^2 \cdot \text{mg Chl}^{-1}$) defined in relation to the actual spectral composition of *in situ* light, photosynthetically usable radiation (PUR):

$$\bar{a}_{\phi PUR}^*(z) = \frac{\int_{400nm}^{700nm} a_{\phi}^*(\lambda) \cdot E_0(\lambda, z) d\lambda}{\int_{400nm}^{700nm} E_0(\lambda, z) d\lambda}, \quad [4]$$

where $a_{\phi}^*(\lambda)$ ($\text{m}^2 \cdot \text{mg Chl}^{-1}$) is lipid-soluble absorption by phytoplankton pigments (Fig. 3A), and $E_0(\lambda, z)$ ($\mu\text{mol quanta} \cdot \text{m}^{-2} \cdot \text{s}^{-1}$) is modeled depth- and spectrally dependent scalar *in situ* irradiance (Fig. 3B, black lines). Scalar irradiance is calculated from downwelling photosynthetically active radiation (PAR) that is measured above the surface of the ocean [$E_d(0^+)$, $\mu\text{mol quanta} \cdot \text{m}^{-2} \cdot \text{s}^{-1}$] and propagated through the water column by using spectrally resolved light attenuation models dependent on date, location, and Chl concentration (23–25). This productivity model (Eq. 3) performed well in comparisons with 24-h simulated *in situ* ^{14}C primary productivity measurements in which 24-h productivity, ϕ_m , P_{\max}^b and $\bar{a}_{\phi PUR}^*(z)$ were measured from identical sample bottles ($r^2 = 0.95$, slope = 0.92).

We use the light-limited, photosynthesis-resolving primary productivity model in Eq. 3 to demonstrate the importance of light-limited productivity in response to enhanced iron supply. Approximately 30-s intervals of measured surface PAR from sunrise to sunset on a typical day during the SOFeX cruise were propagated through a 50-m water column (approximate mixed layer depth) at 1-m intervals using light attenuation models (23–25) to produce the family of 100,000 discrete PAR occurrences shown in the histogram in Fig. 4A. Using Eq. 3, the mean values in Table 1, and the histogram of PAR occurrences (Fig. 4A), the absolute amount of primary productivity ($\text{mmol C} \cdot \text{m}^{-2} \cdot \text{d}^{-1}$) were calculated for each discrete PAR wavelength (Fig. 4D). The same variables were used to plot primary productivity versus depth (Fig. 4E). Fig. 4B shows the mean PvsE curve inside and outside the iron-enriched patch for the mean values in Table 1. The difference between the light-limited vs. light-saturated portion of the PvsE curve is clear in Fig. 4B; light-saturated photosynthesis begins at irradiances of $\approx 100 \mu\text{mol quanta} \cdot \text{m}^{-2} \cdot \text{s}^{-1}$ outside the iron-enriched patch. Approx-

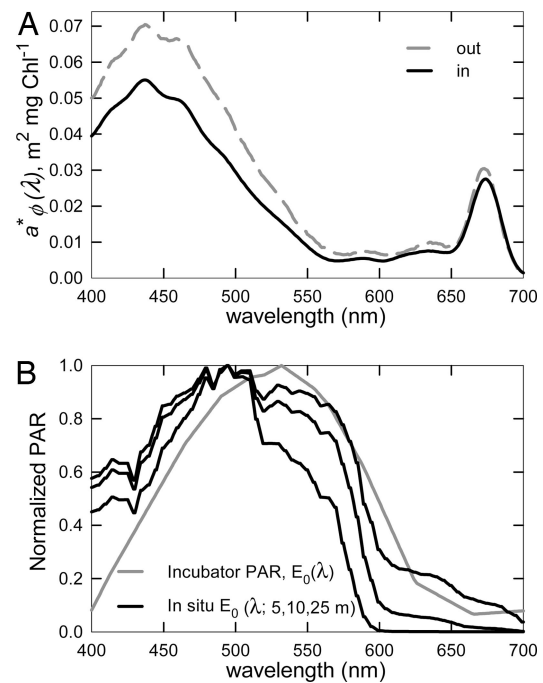


Fig. 3. Absorption coefficient and modeled PAR. (A) Mean wavelength-dependent Chl-specific absorption coefficient, $\alpha^*_{\phi}(\lambda)$, from 400 to 700 nm inside and outside the iron-enriched patch. (B) Modeled individually normalized spectral quality of *in situ* PAR on February 2, 2002, 66°S, 172°W at local noon with a uniform $1 \text{ mg Chl} \cdot \text{m}^{-3}$ from 0- Z_{eu} and PvsE incubator irradiance. The black lines represent modeled PAR, $E_0(\lambda, z)$, at 5, 10, and 25 m representing 60%, 35%, and 9% light levels, respectively. The spectral quality of PAR used for the PvsE incubations, $E_0^{inc}(\lambda)$, is represented by a gray solid line.

imately 83% of the family of PAR occurrences in Fig. 4A occur at light levels $< 100 \mu\text{mol quanta} \cdot \text{m}^{-2} \cdot \text{s}^{-1}$. As a result, the majority of PP_{eu} occurs at low-light intensities (Fig. 4D). For this example, $\approx 58\%$ of the PP_{eu} outside of the iron-enriched patch (total = $19.8 \text{ mmol C} \cdot \text{m}^{-2} \cdot \text{d}^{-1}$) and 66% of the PP_{eu} inside the patch (total = $27.7 \text{ mmol C} \cdot \text{m}^{-2} \cdot \text{d}^{-1}$) occur at light intensities $< 100 \mu\text{mol quanta} \cdot \text{m}^{-2} \cdot \text{s}^{-1}$ (Fig. 4D). More importantly, the large majority of the difference in primary productivity outside and inside the iron-enriched patch occurs at very low light intensities; 50% of the difference occurs at irradiances $< 37 \mu\text{mol quanta} \cdot \text{m}^{-2} \cdot \text{s}^{-1}$ and 84% of the difference occurs at irradiances $< 100 \mu\text{mol quanta} \cdot \text{m}^{-2} \cdot \text{s}^{-1}$ (Fig. 4D).

The relative importance of light-limited productivity only weakly depends on daily irradiance. In Fig. 4, productivity is modeled by using an integrated daily surface irradiance of $16 \text{ mol quanta} \cdot \text{m}^{-2} \cdot \text{d}^{-1}$, which represents a typical irradiance for the SOFeX cruise (range = 9 to $44 \text{ mol quanta} \cdot \text{m}^{-2} \cdot \text{d}^{-1}$). Modeled with the cruise maximum of $44 \text{ mol quanta} \cdot \text{m}^{-2} \cdot \text{d}^{-1}$, 50% of the productivity outside of the iron-enriched patch and 57% of the productivity inside the patch would occur at light intensities $< 100 \mu\text{mol quanta} \cdot \text{m}^{-2} \cdot \text{s}^{-1}$. Fully 50% of the difference in productivity from inside the patch to outside the patch would occur at light intensities $< 48 \mu\text{mol quanta} \cdot \text{m}^{-2} \cdot \text{s}^{-1}$. Regardless of the quantity of total daily irradiance, most photosynthesis in the water column occurs at light-limited irradiances.

Although maximum quantum yield, ϕ_m , has not previously been reported in Southern Ocean iron experiments, all five Southern Ocean bloom-forming mesoscale iron additions conducted between 1999 and 2004 resulted in increased photosynthetic competency as measured by variable fluorescence (1, 2, 26–28). The PvsE experiment results reported here are similar to those made during a 2000 mesoscale iron enrichment exper-

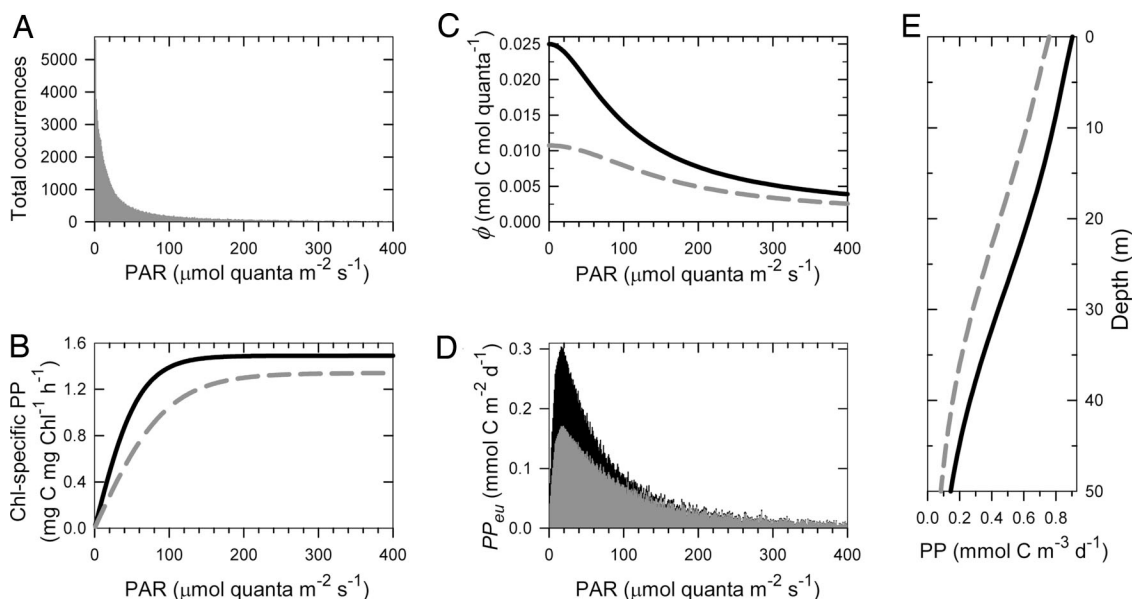


Fig. 4. Modeled productivity and irradiance. (A) Histogram of $\approx 100,000$ total occurrences of PAR at a given PAR. Less than 3% of the total discrete PAR measurements are $>400 \mu\text{mol quanta}\cdot\text{m}^{-2}\cdot\text{s}^{-1}$. (B) Average Chl-specific primary production vs. irradiance inside (black solid line) and outside (gray dashed line) the iron-enriched patch generated from parameters in Table 1. (C) Quantum yield (ϕ_m) vs. PAR inside (black solid) and outside (gray dashed) the iron-enriched patch. (D) Total primary productivity within the euphotic zone (PP_{eu}) at given PAR values inside (black) and outside (gray) the iron-enriched patch. (E) Primary productivity in D plotted vs. depth. Light attenuation and primary productivity was modeled with $\text{Chl} = 0.5 \text{ mg}\cdot\text{m}^{-3}$ from 0 to 50 m for both the control and iron-replete model run to isolate the effect of Chl on primary production; $0.5 \text{ mg}\cdot\text{m}^{-3}$ was chosen as an approximation of the mean Chl concentration in the Southern Ocean poleward of the southern boundary of the Antarctic Circumpolar Current. A 50-m water column was chosen because it represents a typical mixed layer depth and euphotic zone depth in the study area.

iment in the Atlantic sector of the Southern Ocean (EisenEx; ref., 28). “During EisenEx, we observed no general inside/outside difference in P_{max}^b , whereas α^b was slightly higher inside the Fe-enriched patch” (28). Also, one of the first iron-enrichment experiments conducted in the equatorial Pacific saw similar results; iron-induced increases in ϕ_m were not accompanied by significant increases in P^b , Chl-normalized primary production ($\text{mmol C}\cdot\text{mg Chl}^{-1}\cdot\text{d}^{-1}$) (29).

The 5-fold increases in PP_{eu} and 9-fold increases in Chl measured during the SOFeX iron addition were not accompanied by a significant increase in P_{max}^b . Instead, biomass and productivity increases were driven by 2-fold increases in ϕ_m and α^b . Any primary productivity model that does not incorporate variability in light-limited production will fail to reproduce the development of an iron-induced bloom because the physiological driver of the productivity increase (ϕ_m and α^b) in such a model is a constant rather than a variable. Primary productivity algorithms that resolve the variability of light-limited photosynthesis are necessary to model iron effects in the Southern Ocean and, we hypothesize, other iron-regulated regions of the world ocean. Primary productivity models that account for variability in light-limited photosynthesis will better reproduce the effects of natural background and episodic iron inputs.

Materials and Methods

Chl was determined by fluorometric methods and HPLC. Water samples were filtered in parallel onto 25-mm Whatman glass fiber filters (GF/F, nominally a $0.7\text{-}\mu\text{m}$ size fraction) and 5- and $20\text{-}\mu\text{m}$ Poretics polycarbonate filters. Fresh samples were extracted in 90% acetone at -20°C for 24–30 h (30) and quantified by using a Turner Designs fluorometer (31, 32). A complete suite of phytoplankton pigments were also analyzed from frozen samples following the procedures described by Bidigare *et al.* (33).

Maximum quantum yield was determined with measurements of phytoplankton absorption and PvsE experiments. Particulate matter was collected by filtering 0.5–4 liters of upper mixed layer sample water through 25-mm GF/F glass fiber filters, with greater volumes filtered for low biomass waters. Spectral absorption coefficients were measured with a dual beam spectro-

photometer. Diffuse coefficients for total particulate matter were calculated by using the equations described in the National Aeronautics and Space Administration Ocean Optics Protocols (34) and by Mitchell (35). Methanol was used to extract pigments from the filtered sample, and the depigmented filter was then measured to estimate detrital absorption (36). The difference between the two measurements nominally represents lipid-soluble absorption by phytoplankton pigments [$a_{\phi}^*(\lambda)$] (Fig. 3A). The mean Chl-specific absorption coefficient normalized to incubation irradiance ($\bar{a}_{\phi_{INC}}^*$, $\text{m}^2\cdot\text{mg Chl}^{-1}$) is calculated as in Eq. 4 with the exception that $E_0(\lambda, z)$ is replaced with $E_0^{inc}(\lambda)$. $E_0^{inc}(\lambda)$ is the spectrally dependent scalar irradiance of incubation and does not include UV radiation (Fig. 3B, gray solid line).

PvsE curves were derived from ^{14}C uptake measurements after 2-h incubations in temperature-controlled blue light incubators, modified from the design of Jassby and Platt (37). Each incubator held 12 22-ml polyethylene scintillation vials in which natural seawater samples were exposed to different light treatments of PAR. Irradiance was supplied from the bottom of incubation vessels by using a 250-W tungsten-halogen slide projector lamp (Gray ENH), spectrally modified by using a heat mirror, a broad band cool mirror (Optical Coating Laboratory), and blue stage-lighting screens (Cinemills M144). Light intensity was modified by using neutral density screening. Samples were inoculated with 10–50 MBq of $\text{NaH}^{14}\text{CO}_3$ and incubated for 2 h. The incubator vials were cleaned and ^{14}C was prepared according to Fitzwater *et al.* (38).

The Chl-specific maximal photosynthetic rate (P_{max}^b) was estimated by using a nonlinear, least-squares routine (39). The maximum Chl-specific light utilization coefficient [α^b , $\text{mg C}\cdot\text{mg Chl}^{-1}\cdot\text{h}^{-1}\cdot(\mu\text{mol quanta}\cdot\text{m}^{-2}\cdot\text{s}^{-1})^{-1}$] was determined following Johnson and Barber (40). The light-saturation index (E_k , $\mu\text{mol quanta}\cdot\text{m}^{-2}\cdot\text{s}^{-1}$) is the quotient of P_{max}^b and α^b . Maximum quantum yield of carbon uptake (ϕ_m , $\text{mol C}\cdot\text{mol quanta}^{-1}$) was calculated from α^b and $\bar{a}_{\phi_{INC}}^*$:

$$\phi_m = \frac{\alpha^b}{43.2\bar{a}_{\phi_{INC}}^*}, \quad [5]$$

where 43.2 converts seconds to hours, milligrams to mols, and micromols to mols. It is important to note that ϕ_m can be used to describe the ϕ_m of a single phytoplankton cell, in which case the theoretical ϕ_m is 0.125. Here, we use ϕ_m to describe the ϕ_m of the *in situ* mixed phytoplankton assemblage that depends on irradiance, nutrients, and temperature and is unlikely to approach the theoretical maximum of $0.125 \text{ mol C}\cdot\text{mol quanta}^{-1}$. The range of ϕ_m in this

study (0.006 to 0.040 mol C-mol quanta⁻¹; Table 1) is in line with near surface ϕ_m measurements made in the Atlantic Sector of the Southern Ocean (0.006–0.027 mol C-mol quanta⁻¹) (41).

ACKNOWLEDGMENTS. We thank the entire SOFeX group, the crew and officers of RV Revelle, RV Melville, and U.S. Coast Guard ice breaker Polar Star, and members of the primary production team (Liza Delizo, Anna Hilding, Chrissy Van Hilst, Jacques Oliver, Jill Peloquin, and David Stuebe).

1. Coale KH, et al (2004) Southern ocean iron enrichment experiment: Carbon cycling in high- and low-Si waters. *Science* 304:408–414.
2. Boyd PW, et al (2007) Mesoscale iron enrichment experiments 1993–2005: Synthesis and future directions. *Science* 315:612–617.
3. Barber RT, Hiscock MR (2006) A rising tide lifts all phytoplankton: Growth response of other phytoplankton taxa in diatom-dominated blooms. *Global Biogeochem Cycles* 20:GB4503.
4. Lance VP, et al (2007) Primary productivity, differential size fraction and pigment composition responses in two Southern Ocean *in situ* iron enrichments. *Deep-Sea Res* 54:747–773.
5. Peloquin JA, Smith WO (2006) The role of phytoplankton size on photochemical recovery during the Southern Ocean iron experiment. *J Phycol* 42:1016–1027.
6. Martin JH et al. (1994) Testing the iron hypothesis in ecosystems of the equatorial Pacific Ocean. *Nature* 371:123–129.
7. Greene RM, Geider RJ, Kolber Z, Falkowski PG (1992) Iron-induced changes in light harvesting and photochemical energy-conversion processes in eukaryotic marine algae. *Plant Physiol* 100:565–575.
8. Blackman FF (1905) Optima and limiting factors. *Ann Bot* 19:281–295.
9. Kolber ZS, et al (1994) Iron limitation of phytoplankton photosynthesis in the equatorial Pacific Ocean. *Nature* 371:145–149.
10. Geider RJ, Osborne BA (1992) *Algal Photosynthesis: The Measurement of Algal Gas Exchange Current Phycology* (Chapman & Hall, New York), Vol 2.
11. Martin JH (1990) Glacial-interglacial CO₂ change: The iron hypothesis. *Paleoceanography* 5:1–13.
12. Hiscock WT, Millero FJ (2005) Nutrient and carbon parameters during the Southern Ocean iron experiment (SOFeX). *Deep-Sea Res* 52:2086–2108.
13. Fitzwater SE, Johnson KS, Gordon RM, Coale KH, Smith WO (2000) Trace metal concentrations in the Ross Sea and their relationship with nutrients and phytoplankton growth. *Deep-Sea Res II* 47:3159–3179.
14. Johnson KS, Gordon RM, Coale KH (1997) What controls dissolved iron concentrations in the world ocean? *Mar Chem* 57:137–161.
15. Hiscock MR, et al (2003) Primary productivity and its regulation in the Pacific Sector of the Southern Ocean. *Deep-Sea Res II* 50:533–558.
16. Behrenfeld MJ, Falkowski PG (1997) A consumer's guide to phytoplankton primary productivity models. *Limnol Oceanogr* 42:1479–1491.
17. Behrenfeld MJ, Falkowski PG (1997) Photosynthetic rates derived from satellite-based chlorophyll concentration. *Limnol Oceanogr* 42:1–20.
18. Sathyendranath S, Platt T (2007) Spectral effects in bio-optical control on the ocean system. *Oceanologia* 49:5–39.
19. Carr ME, et al (2006) A comparison of global estimates of marine primary production from ocean color. *Deep-Sea Res II* 53:741–770.
20. Platt T, Sathyendranath S (1993) Estimators of primary production for interpretation of remotely sensed data on ocean color. *J Geophys Res-Oceans* 98:14561–14576.
21. Fasham MJR, Flynn KJ, Pondaven P, Anderson TR, Boyd PW (2006) Development of a robust marine ecosystem model to predict the role of iron in biogeochemical cycles: A comparison of results for iron-replete and iron-limited areas, and the SOIREE iron-enrichment experiment. *Deep-Sea Res* 53:333–366.
22. Longhurst A, Sathyendranath S, Platt T, Caverhill C (1995) An estimate of global primary production in the ocean from satellite radiometer data. *J Plankton Res* 17:1245–1271.
23. Bracher AU, Tilzer MM (2001) Underwater light field and phytoplankton absorbance in different surface water masses of the Atlantic sector of the Southern Ocean. *Polar Biol* 24:687–696.
24. Kirk JTO (1984) Dependence of relationship between inherent and apparent optical properties of water on solar altitude. *Limnol Oceanogr* 29:350–356.
25. Morel A (1991) Light and marine photosynthesis: A spectral model with geochemical and climatological implications. *Prog Oceanogr* 26:263–306.
26. Boyd PW, et al (2000) A mesoscale phytoplankton bloom in the polar Southern Ocean stimulated by iron fertilization. *Nature* 407:695–702.
27. Hoffmann LJ, Peekel I, Lochte K, Assmy P, Veldhuis M (2006) Different reactions of Southern Ocean phytoplankton size classes to iron fertilization. *Limnol Oceanogr* 51:1217–1229.
28. Gervais F, Riebesell U, Gorbunov MY (2002) Changes in primary productivity and chlorophyll a in response to iron fertilization in the Southern Polar Frontal Zone. *Limnol Oceanogr* 47:1324–1335.
29. Lindley ST, Barber RT (1998) Phytoplankton response to natural and experimental iron addition. *Deep-Sea Res II* 45:1135–1150.
30. Venrick EL, Hayward TL (1984) Determining chlorophyll on the 1984 CalCOFI surveys. *California Cooperative Oceanic Fisheries Invest Rep* 25:74–79.
31. Holm-Hansen O, Lorenzen CJ, Holmes RW, Strickland JDH (1965) Fluorometric determination of chlorophyll. *J Conseil* 30:3–15.
32. Lorenzen CJ (1966) A method for the continuous measurement of *in vivo* chlorophyll concentration. *Deep-Sea Res* 13:223–227.
33. Bidigare RR, Van Heukelem L, Tree CC (2005) in *Algal Culturing Techniques*, ed Anderson RA (Academic, New York), pp 327–345.
34. Mitchell BG, Kahru M, Weiland J, Stramski M (2003) in *Ocean Optics Protocols for Satellite Ocean Color Sensor Validation*, eds Mueller JL, Fargion GS, McClain CR (National Aeronautics and Space Administration, Greenbelt, MD), Revision 5, Vol V, pp 39–60.
35. Mitchell BG (1990) Algorithms for determining the absorption coefficient of aquatic particulates using the Quantitative Filter Technique (QFT). *Soc Photo-Optical Instrum Eng* 10:137–148.
36. Kishino M, Takahashi M, Okami N, Ichimura S (1985) Estimation of the spectral absorption coefficients of phytoplankton in the sea. *Bull Mar Sci* 37:634–642.
37. Jassby AD, Platt T (1976) Mathematical formulation of the relationship between photosynthesis and light for phytoplankton. *Limnol Oceanogr* 21:540–547.
38. Fitzwater SE, Knauer GA, Martin JH (1982) Metal contamination and its effect on primary production measurements. *Limnol Oceanogr* 27:544–551.
39. Zimmerman RC, SooHoo JB, Kremer JN, D'Argenio DZ (1987) Evaluation of variance approximation techniques for nonlinear photosynthesis-irradiance models. *Mar Biol* 95:209–215.
40. Johnson Z, Barber RT (2003) The low-light reduction in the quantum yield of photosynthesis: Potential errors and bias when calculating the maximum quantum yield. *Photosynth Res* 75:85–95.
41. Bracher AU, Kroon BMA, Lucas MI (1999) Primary production, physiological state, and composition of phytoplankton in the Atlantic Sector of the Southern Ocean. *Mar Ecol-Prog Ser* 190:1–16.

Thoughtful comments by anonymous reviewers, careful stewardship by William H. Schlesinger, and numerous readings by Elaine Barber and Christine Sproat greatly improved this paper. This research was supported by grants from National Science Foundation Chemical and Biological Oceanography Programs and the Office of Polar Programs and the Harvey W. Smith Endowment of Duke University. M.R.H. was supported by Robert Safrin, Harvey W. Smith, and Rachel Carson Graduate Fellowships at Duke University.